Results in Physics 15 (2019) 102732

Contents lists available at ScienceDirect

Results in Physics

journal homepage: www.elsevier.com/locate/rinp

Multi-order quantum beating effect of three-photon temporal interference with nondegenerate fluorescence sources

Ruimin Wang*, Faizan Raza, Renjun Pang, Abubakkar Khan, Habib Ullah, Yanpeng Zhang*

School of Science & Key Laboratory for Physical Electronics and Devices of the Ministry of Education & Shaanxi Key Lab of Information Photonic Technique, Xi'an Jiaotong University, Xi'an 710049, China

ARTICLE INFO

Keywords:
Quantum optical
Quantum beating
Coherent optical effects

ABSTRACT

The multi-order quantum beating effect of three-photon temporal interference generated by three nondegenerate fluorescence sources is studied. The third-order temporal correlation function of three nondegenerate photons results from the superposition of two-photon and three-photon bunching, multi-order quantum beating and temporal interference of three-photon. The simulate results show strong quantum beating and photon bunching behavior. The visibility of interference pattern, and the switching between photon bunching and beating effect can be modulated by the frequency difference, bandwidth of photons and the relative time delay of detectors. Such controllable coherent signal has potential applications as router and logic gate in quantum communication and information processing.

Introduction

The two-photon interference is one of the most important mechanisms for understanding quantum theory and realizing quantum information processing. The first- and second-order interference of two independent light beams has been studied extensively with different light sources, such as coherent light [1–4], thermal light sources [5–7], and nonclassical light sources [8,9]. According to the superposition principle in Feynman's path integral theory [10], two-photon interference is not the interference between two individual photons, but the interference resulting from different Feynman paths [11]. That is, two-photon interference with thermal light is not caused by the statistical correlation of the intensity fluctuations [12]. The two-photon interference with nondegenerate paired photons has also been demonstrated [13]. When two photons are in different frequencies, the two-photon interference can be measured as a quantum beating in time domain [14,15].

The two-photon interference plays an important role in quantum imaging. The first two-photon ghost-imaging experiment was demonstrated by using entangled photon pairs of spontaneous parametric down-conversion in 1995 [16]. After then, it is found that ghost imaging can be realized with chaotic thermal light [12,17]. Compared to two-photon entangled sources, the disadvantage of classical light in ghost imaging is the limited visibility. In principle, the visibility of entangled sources can be as high as 100%, while the visibility of classical light cannot exceed 50% [18]. On the other hand, in order to obtain high visibility, two-photon entangled sources should have low counting rates. Comparatively, the visibility of classical sources is independent of the intensity, which can be very high.

Recently, it is found that high-order interference may help to boost the visibility of classical sources. For three-photon and four-photon interference of two coherent sources, the visibility can be attained 81.8% and 94.4%, respectively [19]. Moreover, the visibility of Hanbury Brown and Twiss (HBT) interference for classical light grows rapidly with the order of interference. It is expected in theory that the visibility of thermal light can achieve 100% by measuring the *N*th-order correlation [20,21]. Multiphoton interference of classical light provides a method to obtain high visibility and counting rates for ghost imaging. However, the main attention has been focused on second-order interference for a long time. Discussions about multiphoton interference are very little until now, and it is only restricted to degenerate photons. High-order interference of nondegenerate photons includes important mechanisms, such as multi-order quantum beating effect. It is useful to realize quantum information processing.

In this paper we present multi-order quantum beating effect generated by third-order temporal interference of three nondegenerate thermal sources. We analyze multi-order quantum beating and three-photon bunching effect at different frequency bandwidth, frequency deference and relative time delay of three fluorescence sources. We adjust the visibility of thermal light imaging by the effect of quantum

* Corresponding authors.
E-mail addresses: wangrm@mail.xjtu.edu.cn (R. Wang), ypzhang@mail.xjtu.edu.cn (Y. Zhang).

https://doi.org/10.1016/j.rinp.2019.102732
Received 12 July 2019; Received in revised form 13 September 2019; Accepted 7 October 2019
Available online 15 October 2019

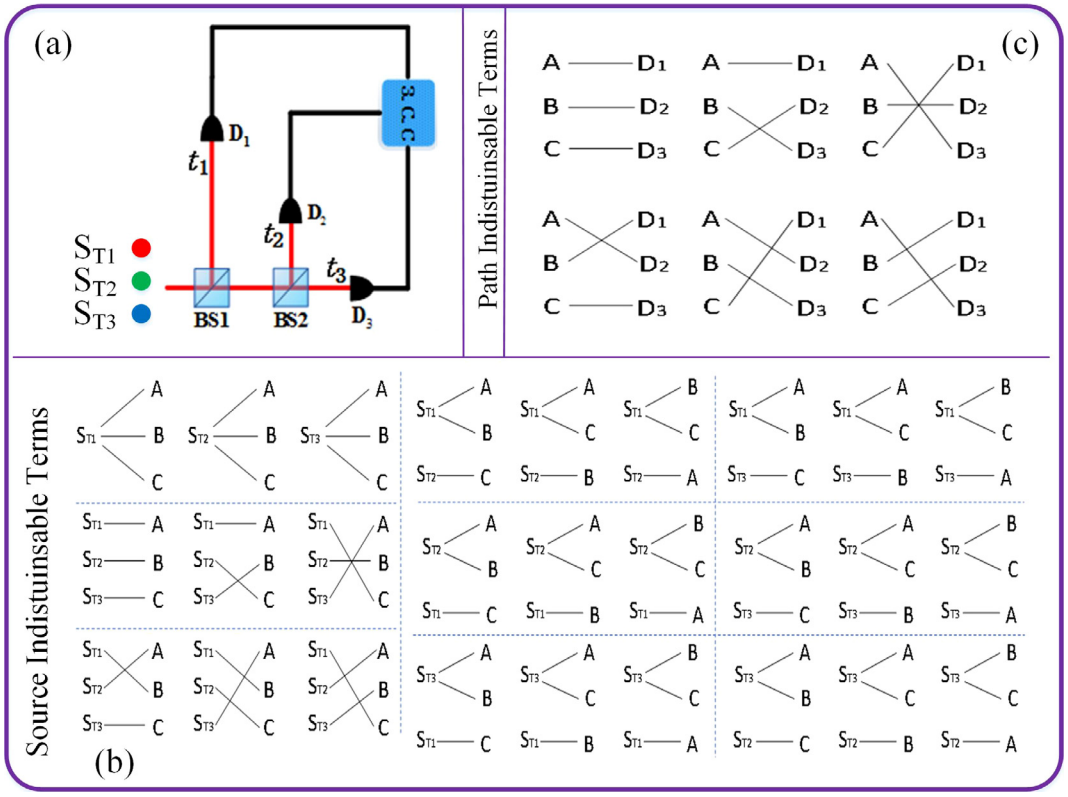

Fig. 1. (a) Experimental setup to measure third-order temporal correlation function of thermal sources. S_{T1}, S_{T2} and S_{T3} are three independent fluorescence sources. D_1, D_2 and D_3 are three single-photon detectors. BS_1: 1:2 beam splitter. BS_2: 1:1 beam splitter. CCC: three-photon coincidence count detection system. (b) Twenty-seven different cases to emit three photons by three independent sources. (c) Three independent photons A, B, C have six different ways to trigger three-photon detection event.

beating.

Theoretical model

We will discuss third-order interference of three fluorescence sources based on the superposition principle in Feynman's path integral theory. Fig. 1(a) is the experimental setup for measuring third-order temporal correlation function. Three independent fluorescence beams pass through non-polarizing beam splitters BS_1 and BS_2, and then be detected by three photon detectors D_1, D_2 and D_3, respectively. The distances between the sources and three detectors are all equal. The output of the detectors is input into the three-photon coincidence count system. For simplicity, the polarizations and intensities in three paths are assumed to be the same.

The superposition principle in Feynman's path integral theory is based on the indistinguishability of different alternatives. Fig. 1(b) shows that there are twenty-seven different cases to emit three photons by three independent sources, which are named as source indistinguishable terms. The first one is all three photons emitted by S_{T1}. The second one is photon A emitted by S_{T1}, photon B emitted by S_{T2}, and photon C emitted by S_{T3}, respectively. Other possibilities of source indistinguishable terms are shown in Fig. 1(b). Although the frequencies of the photons emitted by three independent sources are different, these different alternatives can be regard as indistinguishable if the time measurement uncertainty of the detection system is less than $1/\omega_{ij}$ [22], where $\omega_{ij}$is the frequency difference of two sources. In each case, there are six different ways to trigger a three-photon coincidence count (as shown in Fig. 1(c)), which are defined as path entanglement or indistinguishable terms. For example, $A \rightarrow D_1$, $B \rightarrow D_2$, $C \rightarrow D_3$ means photon A triggers detectors D_1, photon B triggers detectors D_2 and photon C triggers detectors D_3, respectively. The combine effect of source and path indistinguishable terms results in interference of three photons.

Three-photon interference is the result of the coherent superposition of three-photon probability amplitudes, which depend on indistinguishable ways to trigger a three-photon coincidence count. The jth detected three-photon probability distribution is

$$P_j^{(3)}(\vec{r}_1, t_1, \vec{r}_2, t_2, \vec{r}_3, t_3)=|P_{1j}(\vec{r}_1, t_1, \vec{r}_2, t_2, \vec{r}_3, t_3) + P_{2j}(\vec{r}_1, t_1, \vec{r}_2, t_2, \vec{r}_3, t_3) + \ldots\ldots+P_{27j}(\vec{r}_1, t_1, \vec{r}_2, t_2, \vec{r}_3, t_3)|^2 \quad (1)$$

$P_{ij}(\vec{r}_1, t_1, \vec{r}_2, t_2, \vec{r}_3, t_3)$ $(i=1,2,\ldots\ldots,27)$ correspond to twenty-seven different cases of source indistinguishable terms as shown in Fig. 1(b). In each case, there are six path indistinguishable terms (as shown in Fig. 1(c)). For example, $P_{1j}(\vec{r}_1, t_1, \vec{r}_2, t_2, \vec{r}_3, t_3)$, $P_{2j}(\vec{r}_1, t_1, \vec{r}_2, t_2, \vec{r}_3, t_3)$ can be written as

$$\begin{aligned} P_{1j}(\vec{r}_1, t_1, \vec{r}_2, t_2, \vec{r}_3, t_3) = {} & e^{i\left(\varphi_{1jA}+\frac{\pi}{2}\right)}K_{11}e^{i\left(\varphi_{1jB}+\frac{\pi}{2}\right)}K_{12}e^{i\varphi_{1jC}}K_{13} \\ & + e^{i\left(\varphi_{1jA}+\frac{\pi}{2}\right)}K_{11}e^{i\varphi_{1jB}}K_{13}e^{i\left(\varphi_{1jC}+\frac{\pi}{2}\right)}K_{12} \\ & + e^{i\varphi_{1jA}}K_{13}e^{i\left(\varphi_{1jB}+\frac{\pi}{2}\right)}K_{12}e^{i\left(\varphi_{1jC}+\frac{\pi}{2}\right)}K_{11} \\ & + e^{i\left(\varphi_{1jA}+\frac{\pi}{2}\right)}K_{12}e^{i\left(\varphi_{1jB}+\frac{\pi}{2}\right)}K_{11}e^{i\varphi_{1jC}}K_{13} \\ & + e^{i\left(\varphi_{1jA}+\frac{\pi}{2}\right)}K_{12}e^{i\varphi_{1jB}}K_{13}e^{i\left(\varphi_{1jC}+\frac{\pi}{2}\right)}K_{11} \\ & + e^{i\varphi_{1jA}}K_{13}e^{i\left(\varphi_{1jB}+\frac{\pi}{2}\right)}K_{11}e^{i\left(\varphi_{1jC}+\frac{\pi}{2}\right)}K_{12} \end{aligned} \quad (2)$$

$$\begin{aligned} P_{2j}(\vec{r}_1, t_1, \vec{r}_2, t_2, \vec{r}_3, t_3) = {} & e^{i\left(\varphi_{2jA}+\frac{\pi}{2}\right)}K_{21}e^{i\left(\varphi_{2jB}+\frac{\pi}{2}\right)}K_{22}e^{i\varphi_{2jC}}K_{23} \\ & + e^{i\left(\varphi_{2jA}+\frac{\pi}{2}\right)}K_{21}e^{i\varphi_{2jB}}K_{23}e^{i\left(\varphi_{2jC}+\frac{\pi}{2}\right)}K_{22} \\ & + e^{i\varphi_{2jA}}K_{23}e^{i\left(\varphi_{2jB}+\frac{\pi}{2}\right)}K_{22}e^{i\left(\varphi_{2jC}+\frac{\pi}{2}\right)}K_{21} \\ & + e^{i\left(\varphi_{2jA}+\frac{\pi}{2}\right)}K_{22}e^{i\left(\varphi_{2jB}+\frac{\pi}{2}\right)}K_{21}e^{i\varphi_{2jC}}K_{23} \\ & + e^{i\left(\varphi_{2jA}+\frac{\pi}{2}\right)}K_{22}e^{i\varphi_{2jB}}K_{23}e^{i\left(\varphi_{2jC}+\frac{\pi}{2}\right)}K_{21} \\ & + e^{i\varphi_{2jA}}K_{23}e^{i\left(\varphi_{2jB}+\frac{\pi}{2}\right)}K_{21}e^{i\left(\varphi_{2jC}+\frac{\pi}{2}\right)}K_{22} \end{aligned} \quad (3)$$

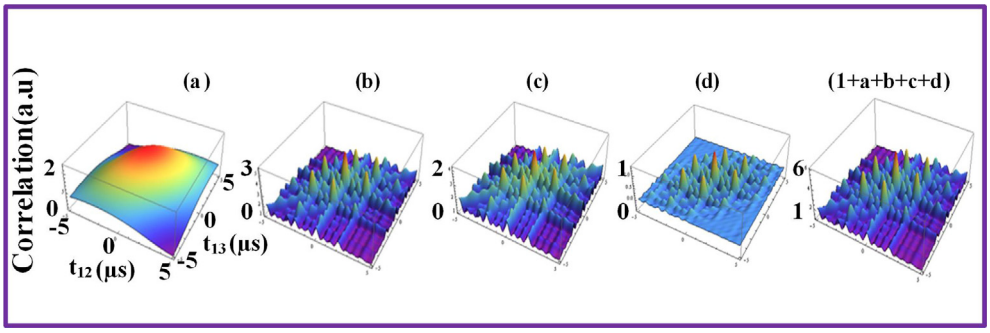

Fig. 2. The simulation results of each term in Eq. (6). The wavelengths of three sources are set at 610 nm, 575 nm and 575.5 nm, respectively.

Other terms in Eq. (1) are defined similarly. Where $\varphi_{1\,j_{A,B,C}}(\varphi_{2\,j_{A,B,C}})$ is the initial phase of photon A (B, C) emitted by source $S_{T1}(S_{T2})$ in the jth detected photon pair. The extra phase $\pi/2$ is due to the photon reflected by the beam splitter will gain an extra phase comparing to the transmitted one. For the point thermal sources, Feynman's photon propagator is defined as

$$K_{\alpha\beta} = \frac{\exp[-i(\vec{k}_{\alpha\beta}\cdot\vec{r}_{\alpha\beta} - \omega_\alpha t_\beta)]}{r_{\alpha\beta}} \tag{4}$$

$\vec{k}_{\alpha\beta}$ and $\vec{r}_{\alpha\beta}$ are the wave and position vectors of the photon emitted by $S_{T\alpha}$ and detected at D_β, respectively. ω_α and t_β are the frequency and time for the photon that is emitted by $S_{T\alpha}$ and detected at D_β, respectively ($\alpha, \beta = 1, 2, 3$). The final three-photon probability distribution is the sum of all detected probability distribution

$$\begin{aligned} P^{(3)}(\vec{r}_1, t_1, \vec{r}_2, t_2, \vec{r}_3, t_3) &= \sum_j P_j^{(3)}(\vec{r}_1, t_1, \vec{r}_2, t_2, \vec{r}_3, t_3) \\ &= \langle |\mathrm{P}_{1j}(\vec{r}_1, t_1, \vec{r}_2, t_2, \vec{r}_3, t_3) + \mathrm{P}_{2j}(\vec{r}_1, t_1, \vec{r}_2, t_2, \vec{r}_3, t_3) \\ &\quad + \ldots\ldots + \mathrm{P}_{27j}(\vec{r}_1, t_1, \vec{r}_2, t_2, \vec{r}_3, t_3)|^2 \rangle \end{aligned} \tag{5}$$

where $\langle \ldots \rangle$ is ensemble average of all detected three-photon probability distribution. Since three thermal sources are independent, the ensemble average of phase $\langle e^{i\varphi_{\alpha\, j\beta} - \varphi_{\mu\, j\nu}} \rangle$ ($\alpha = 1, 2, 3$, $\beta = A, B, C$) equal zero. To simplify the calculation of temporal correlation, we assume that the frequency bandwidths of three sources are same, $\Delta\omega_1 = \Delta\omega_2 = \Delta\omega_3 = \Delta\omega$, and three detectors have an equal distance from sources. Substituting Eq. (4) into Eq. (5), the normalized three-order temporal correlation function can be deduced as

$$P^{(3)}(t_1, t_2, t_3) = 1 + a + b + c + d \tag{6}$$

where

$$\begin{aligned} a = {} & \frac{1}{3}\sin c^2\left[\frac{\Delta\omega(t_1 - t_2)}{2}\right] + \frac{1}{3}\sin c^2\left[\frac{\Delta\omega(t_2 - t_3)}{2}\right] + \frac{1}{3} \\ & \sin c^2\left[\frac{\Delta\omega(t_3 - t_1)}{2}\right] + \frac{2}{9}\sin c\left[\frac{\Delta\omega(t_1 - t_2)}{2}\right]\sin c\left[\frac{\Delta\omega(t_2 - t_3)}{2}\right] \\ & \sin c\left[\frac{\Delta\omega(t_3 - t_1)}{2}\right] \end{aligned} \tag{7}$$

$$\begin{aligned} b = {} & \frac{2}{9}\sin c^2\left[\frac{\Delta\omega(t_1 - t_2)}{2}\right] \times \{\cos[(t_1 - t_2)(\omega_1 - \omega_2)] \\ & + \cos[(t_1 - t_2)(\omega_1 - \omega_3)] + \cos[(t_1 - t_2)(\omega_2 - \omega_3)]\} \\ & + \frac{2}{9}\sin c^2\left[\frac{\Delta\omega(t_2 - t_3)}{2}\right] \times \{\cos[(t_2 - t_3)(\omega_1 - \omega_2)] \\ & + \cos[(t_2 - t_3)(\omega_1 - \omega_3)] + \cos[(t_2 - t_3)(\omega_2 - \omega_3)]\} \\ & + \frac{2}{9}\sin c^2\left[\frac{\Delta\omega(t_3 - t_1)}{2}\right] \times \{\cos[(t_3 - t_1)(\omega_1 - \omega_2)] \\ & + \cos[(t_3 - t_1)(\omega_1 - \omega_3)] + \cos[(t_3 - t_1)(\omega_2 - \omega_3)]\} \end{aligned} \tag{8}$$

$$\begin{aligned} c = {} & \frac{4}{27}\sin c\left[\frac{\Delta\omega(t_1 - t_2)}{2}\right]\sin c\left[\frac{\Delta\omega(t_2 - t_3)}{2}\right]\sin c\left[\frac{\Delta\omega(t_3 - t_1)}{2}\right] \\ & \times \{\cos[(t_1 - t_2)(\omega_1 - \omega_2)] + \cos[(t_2 - t_3)(\omega_1 - \omega_2)] \\ & + \cos[(t_3 - t_1)(\omega_1 - \omega_2)] + \cos[(t_1 - t_2)(\omega_1 - \omega_3)] \\ & + \cos[(t_2 - t_3)(\omega_1 - \omega_3)] + \cos[(t_3 - t_1)(\omega_1 - \omega_3)] \\ & + \cos[(t_1 - t_2)(\omega_2 - \omega_3)] + \cos[(t_2 - t_3)(\omega_2 - \omega_3)] \\ & + \cos[(t_3 - t_1)(\omega_2 - \omega_3)]\} \end{aligned} \tag{9}$$

$$\begin{aligned} d = {} & \frac{2}{27}\sin c\left[\frac{\Delta\omega(t_1 - t_2)}{2}\right]\sin c\left[\frac{\Delta\omega(t_2 - t_3)}{2}\right]\sin c\left[\frac{\Delta\omega(t_3 - t_1)}{2}\right] \\ & \times \{\cos[\omega_1(t_1 - t_2) + \omega_2(t_2 - t_3) + \omega_3(t_3 - t_1)] \\ & + \cos[\omega_1(t_1 - t_2) + \omega_3(t_2 - t_3) + \omega_2(t_3 - t_1)] \\ & + \cos[\omega_2(t_1 - t_2) + \omega_1(t_2 - t_3) + \omega_3(t_3 - t_1)] \\ & + \cos[\omega_2(t_1 - t_2) + \omega_3(t_2 - t_3) + \omega_1(t_3 - t_1)] \\ & + \cos[\omega_3(t_1 - t_2) + \omega_1(t_2 - t_3) + \omega_2(t_3 - t_1)] \\ & + \cos[\omega_3(t_1 - t_2) + \omega_2(t_2 - t_3) + \omega_1(t_3 - t_1)]\} \end{aligned} \tag{10}$$

In above equations $\sin c(x) = \sin x/x$, $t_i (i = 1, 2, 3)$ is the registration time of the photo detection event at D_1, D_2 and D_3, respectively. Fig. 2 shows the simulation results of each term in Eq. (6). The pattern of term a (Eq. (7)) shows a dominant peak which results from the superposition of three two-photon bunching and a three-photon bunching. Term b (Eq. (8)) is the second-order frequency beating term of two photons. c (Eq. (9)) is the third-order frequency beating term. d (Eq. (10)) is the third-order temporal interference term of three photon among different quantum paths. One can see that the patterns of term b, c and d are almost same except for amplitude difference. They all show six secondary peaks around the dominant peak. The contribution of term d is smaller than other terms. The combine simulation result of third-order correlation function $P^{(3)}(t_1, t_2, t_3)$ includes two-photon and three-photon bunching, multi-order frequency beating and temporal interference of three-photon. Therefore, we can say that the third-order correlated pattern includes all information in the pattern of second-order correlation. From above equations, one can predict that, the term $\cos(t_i - t_j)(\omega_i - \omega_j)$ $(i, j = 1, 2, 3)$ is responsible for introducing interference caused by frequency beating and times difference due to path difference reaching coincident counter. When $t_1 = t_2 = t_3$, correlation function achieves its maximum value $P^{(3)} = 6$. Accordingly, the visibility of correlation pattern is $v = (I_{\max} - I_{\min})/(I_{\max} + I_{\min}) \approx 71\%$, which exceeds the 50% thermal sources limit of second-order interference. Where $I_{\max}(I_{\min})$ is the maximal (minimal) value of the measured interference pattern. If three photons are degenerate, frequency beating will disappear, this case is three-photon bunching. Eq. (6) is simplified as

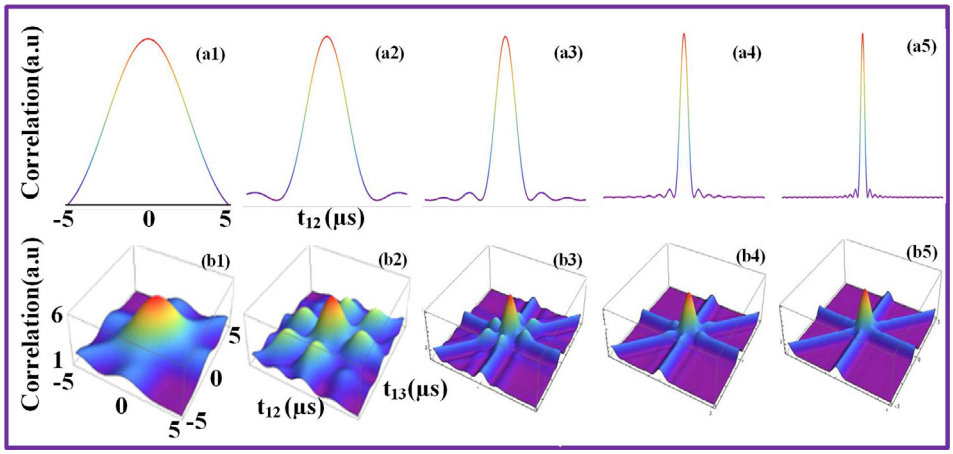

Fig. 3. The calculated third-order temporal correlation functions of three photons by varying bandwidth $\Delta\omega$ of all sources from 0 MHz (1) to 10 MHz (5). (a) The conditional third-order correlation function $P^{(3)}(t_1, t_2, t_3)$ when the detector D3 is fixed at $t_3 = 0$. (b) The 3-D third-order correlation function as the function of relative time delay t_{12} and t_{13}. The wavelengths of three sources are set at 574.5 nm, 575 nm and 575.5 nm, respectively.

$$P^{(3)}(t_1,t_2,t_3) \propto 1 + \sin c^2\frac{\Delta\omega(t_1-t_2)}{2} + \sin c^2\frac{\Delta\omega(t_2-t_3)}{2} + \sin c^2\frac{\Delta\omega(t_3-t_1)}{2} + 2\sin c\frac{\Delta\omega(t_1-t_2)}{2}\sin c\frac{\Delta\omega(t_2-t_3)}{2}\sin c\frac{\Delta\omega(t_3-t_1)}{2} \quad (11)$$

Simulated results and discussions

We simulate third-order temporal correlation function of three nondegenerate sources by employing Eqs. (6)–(10). The multi-order fluorescence (FL) of nitrogen vacancy center in diamond [23,24] is chosen as nondegenerate thermal sources. The third-order temporal correlation function is depicted as the function of variables t_{ij}, where $t_{ij} = t_i - t_j (i, j = 1, 2, 3)$ is the relative time delay between two detectors. We will analyze the dependence of third-order temporal correlation on frequency difference, bandwidth of thermal sources and the relative time delay of detectors.

We first consider the effect of three-photon bunching. Fig. 3 depicts the calculated third-order temporal correlation functions of three thermal sources by varying bandwidth $\Delta\omega$ of thermal sources from 0 MHz to 10 MHz. When fix the time position of detector D_3 at $t_3 = 0$, the conditional third-order correlation function can be obtained. Fig. 2(a) shows the conditional third-order correlation function as the function of relative time delay t_{12}. Fig. 2(b) is the 3-D third-order correlation function as the function of the relative time delay t_{12} and t_{13}. In the simulation, the frequencies of three thermal sources are near degenerate, the frequency beating term $\cos(t_i - t_j)(\omega_i - \omega_j)$ is approximately equal to constant 1. So, the third-order correlation function mainly shows three-photon bunching peak. Quantum beating effect almost disappears. When three detectors are in symmetrical time position, the three-photon amplitudes interfere constructively, the third-order correlation function achieves its maximum value $P^{(3)} = 6$. As the bandwidth $\Delta\omega$ of three sources is gradually increased, the period of the term $\sin c[\Delta\omega(t_i - t_j)]$ in Eq. (7) gradually decreases. As a result, the bunching peak becomes more and more sharp. Simultaneously, the secondary peaks around the dominant peak become weaker.

Now we focus on the quantum beating effect of three photons. Fig. 4 shows conditional third-order temporal correlation functions in the direction of t_{12} when time t_3 is fixed. Correlation curves are plotted by varying the wavelength of FL source S_{T1} from 575 nm to 637 nm, and fixing the others at 575 nm and 575.5 nm, respectively. When three FL sources are near degenerate (Fig. 4(a1)), photon bunching effect is dominant, correlation curve only shows a dominant peak which caused by three photon bunching. As frequency of FL source S_{T1} increases, the second- and third-order frequency beating term b and c, as well as the interference term d of three nondegenerate photons become more and more important in three-order temporal correlation function Eq. (6). We can see the dominant peak becomes sharper, simultaneously, the secondary peaks enhance. The secondary peaks can be attributed to quantum path interference between two-photon bunching and three-photon bunching. With the frequency of source S_{T1} further increasing, the envelope of the correlation peak shows fast interference fringes and the number of fringes increases dramatically. This result is caused by the combined effect of three-photon bunching and second- and third-order quantum beating. From Eqs. (8) to (9) we can see that both second- and third-order quantum beating are determined by $\cos(t_i - t_j)(\omega_i - \omega_j)$. The oscillation frequency of secondary peaks is proportional to the frequency deference $(\omega_i - \omega_j)$ of three nondegenerate photons. So the number of fringes increases with the increasing of frequency deference.

Fig. 5 shows the 3-D third-order correlation function when t_2 and t_3 are scanned. Other conditions are as same as Fig. 4. With increasing of the frequency deference $(\omega_i - \omega_j)$, we find the number and the intensity of small peaks around the dominant peak increases and the intensity of the bunching peak is suppressed due to conservation of energy. From Eqs. (6) to (10) we can know the third-order correlation function is modulated by the frequency beating term $\cos(t_i - t_j)(\omega_i - \omega_j)$. When $(\omega_i - \omega_j)$ is small, the period of $\cos(t_i - t_j)(\omega_i - \omega_j)$ is large, so correlation curve only shows a bunching peak. As $(\omega_i - \omega_j)$ increases, the period of $\cos(t_i - t_j)(\omega_i - \omega_j)$ becomes smaller. Six secondary peaks around the dominant peak appear, which result from second- and third-order quantum beating term in Eqs. (8) and (9). Further increasing frequency deference $(\omega_i - \omega_j)$, the period of $\cos(t_i - t_j)(\omega_i - \omega_j)$ gradually decreases. As a result, six small peaks continue to split around each secondary peak. Finally, the correlation curve forms a nest-like structure. At the same time, the frequency beating term $\cos(t_i - t_j)(\omega_i - \omega_j)$ also modulate the intensity of the bunching peak. With the increasing of frequency deference, the intensity of the secondary peaks increases, and the intensity differences between the dominant peak and the secondary peaks become more and more small (as shown in Fig. 5(a7-8)). It means that the visibility of third order thermal light interference is reduced. This result suggests that we can adjust the visibility of interference pattern by the effect of frequency beating. Furthermore, such splitting signal can be used as switching and router in quantum communication.

Finally, we analyze the time position of dominant peak changing with the time delay of detectors, which is aimed to verify the existence of point-to-point temporal correspondence between signals. As similar as object and image plane in ghost imaging [17], signals in D1 and

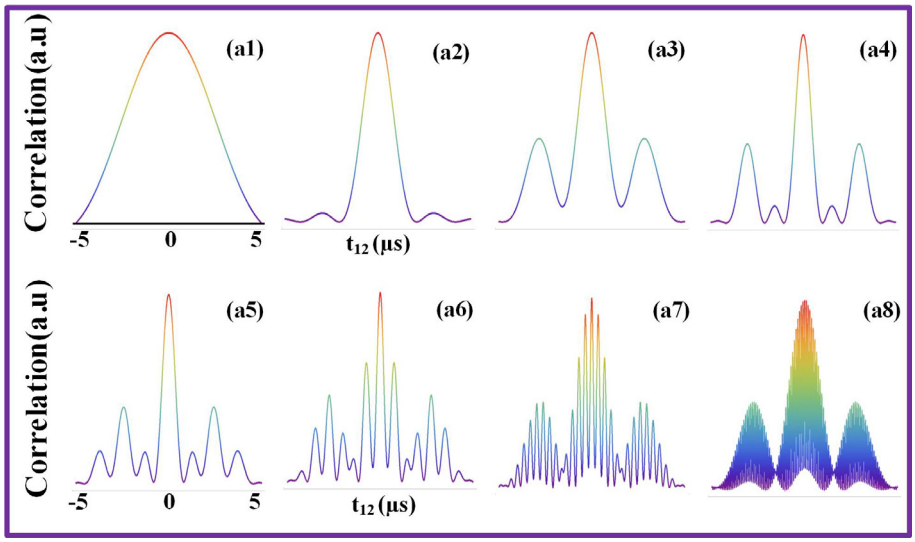

Fig. 4. The conditional third-order temporal correlation functions of three nondegenerate photons. (a1)-(a8) The wavelength of source S_{T1} change from 575 nm to 637 nm, and the wavelengths of source S_{T2} and S_{T3} are fixed at 575 nm and 575.5 nm, respectively.

D2(D3) can be regard as the emission and accepted signals, respectively. Fig. 6(b) shows the third-order temporal correlation functions obtained by selecting time position of detector D1 from $t_1 = -2\mu s$ to $t_1 = 2\mu s$ and other two detector are scanned. For conditional third-order correlation function in Fig. 6(a), time position of detector D3 is further fixed at $t_3 = 0\mu s$. When time position of D1 is set at $t_1 = -2\mu s$, we can see the dominated peak appears at $t_2 = t_3 = -2\mu s$. When time position of D1moved to $t_1 = 0\mu s$, the dominated peak appears at the position $t_2 = t_3 = 0\mu s$. The dominated peak further shifts towards rightward when the position of D1 is fixed at $t_1 = 1\mu s$. With bunching peak shifted with t_1, other smaller interference peaks also change their position with t_1. We can conclude that any shift of time position in emission signal causes a shift of correlation function in accepted signal. The results clearly show point-to-point temporal correspondence between emission and accepted signals. Such results also can be used to realize a transistor switching and a photon bunching NOR logic gate [25].

Conclusion

In conclusion, we study multi-order quantum beating effect by third-order temporal interference of three nondegenerate thermal sources. The third-order temporal correlation function of three nondegenerate thermal sources is derived, which includes two-photon and three-photon bunching, multi-order quantum beating and temporal interference of three-photon. We also simulate third-order temporal correlation function at different frequency, bandwidth of photons and the relative time delay of detectors. The results show strong quantum beating and photon bunching behavior. The conversion between bunching and beating effect is observed by changing frequency deference and bandwidth of photons. It is demonstrated that the visibility of interference pattern can be adjusted by the effect of beating. We also observed that any shift of time position in emission signal causes a shift of correlation peak in accepted signal, which verify point-to-point temporal correspondence between emission and accepted signals. The multi-order quantum beating and the conversion between bunching and beating effect can be used to realize switching, router and NOR logic

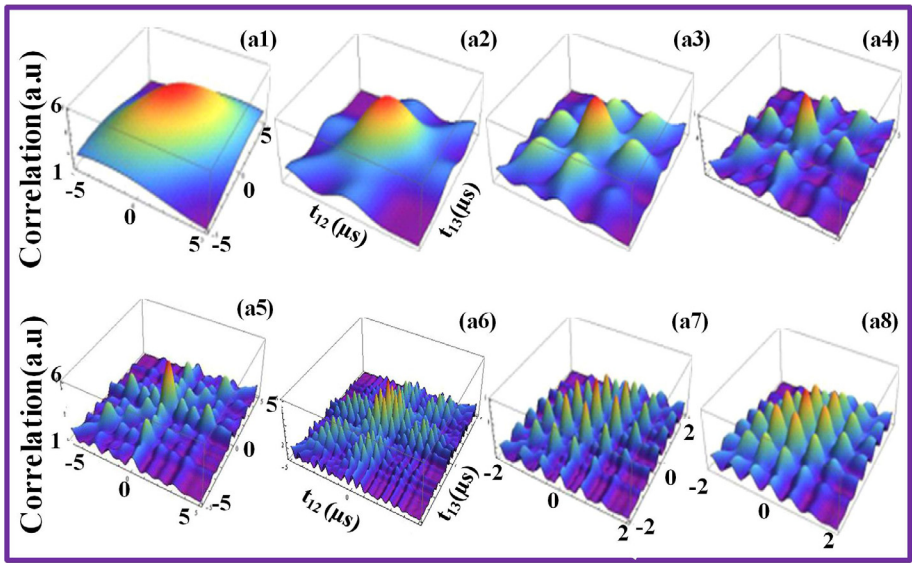

Fig. 5. The 3-D third-order temporal correlation functions of three nondegenerate photons. (a1)-(a8) The wavelength of source S_{T1} change from 575 nm to 637 nm, and the wavelengths of source S_{T2} and S_{T3} are fixed at 575 nm and 575.5 nm, respectively.

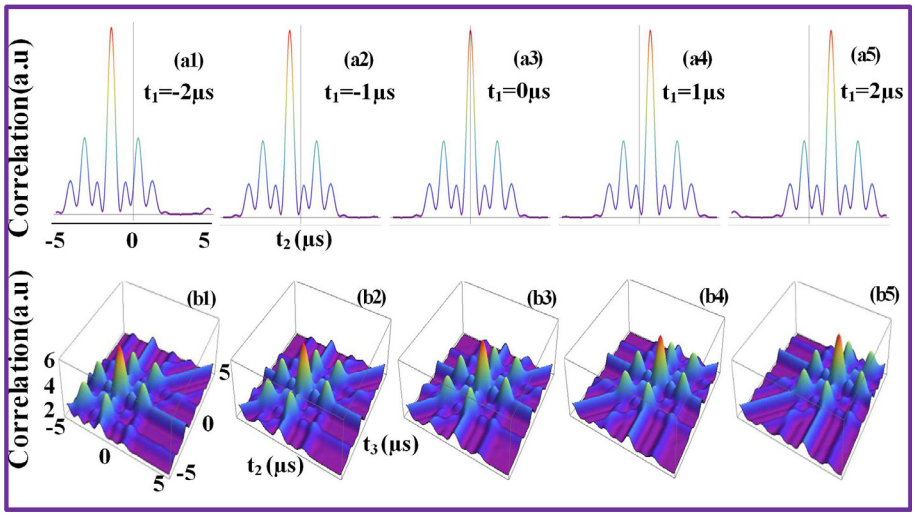

Fig. 6. The third-order temporal correlation functions at different time position of t_1. From (1)-(5), the time position of detector D1 is set at -2, -1, 0, 1 2 μs respectively. (a) The conditional third-order correlation function when the detector D3 is fixed at $t_3 = 0\mu s$ and detector D2 is scanned. (b) The third-order temporal correlation functions when t_2 and t_3 are scanned.

gate in quantum communication. Our studies are helpful to understand higher-order interference of multiple light sources.

Author statement

Yanpeng Zhang has made substantial contributions to the conception and design of the work.

Ruimin Wang has made substantial contributions to analysis, interpretation of data and drafted the manuscript.

Faizan Raza, Renjun Pang, Abubakkar Khan and Habib Ullah have made contributions to the acquisition and analysis of data for the work.

I agree to be accountable for all aspects of the work in ensuring that questions related to the accuracy or integrity of any part of the work are appropriately investigated and resolved.

All persons who have made contributions to the work reported in the manuscript.

Funding

This work was supported by the National Key R&D Program of China (2017YFA0303700, 2018YFA0307500), National Natural Science Foundation of China (61975159, 61605154, 11604256, 11804267, 11904279).

Appendix A. Supplementary data

Supplementary data to this article can be found online at https://doi.org/10.1016/j.rinp.2019.102732.

References

[1] Magyar G, Mandel L. Nature 1963;198:255–6.
[2] Liu JB, Zhang GQ. Opt Commun 2011;284:2658–61.
[3] Kim YS, Slattery O, Kuo PS, Tang X. Phys Rev A 2013;87:063843.
[4] Kim YS, Slattery O, Kuo PS, Tang X. Opt Express 2014;22:3611–20.
[5] Zhai YH, Chen XH, Wu LA. Phys Rev A 2006;74:053807.
[6] Liu JB, Zhou Y, Wang WT, Liu RF, He K, Li FL, et al. Opt Express 2013;16:19209–18.
[7] Liu JB, Zheng HB, Chen H, Zhou Y, Li FL, Xu Z. Opt Express 1878;23(2015):11868–71.
[8] Mandel L. Rev Mod Phys 1999;71:S274–87.
[9] Paul H. Rev Mod Phys 1986;58:209–31.
[10] Feynman RP, Hibbs AR. Quantum mechanics and path integrals. McGraw-Hill Inc; 1965.
[11] Pittman TB, Strekalov DV, Migdall A, Rubin MH, Sergienko AV, Shih YH. Phys Rev Lett 1996;77:1917.
[12] Scarcelli G, Berardi V, Shih Y. Phys Rev Lett 2006;96:063602.
[13] Liu C, Chen JF, Zhang SC, Zhou SY, Kim YH, Loy MMT, et al. Phys Rev A 2012;85:021803.
[14] Legero T, Wilk T, Kuhn A, Rempe G. Appl Phys B 2003;77:797–802.
[15] Legero T, Wilk T, Hennrich M, Rempe G, Kuhn A. Phys Rev Lett 2004;93:070503.
[16] Pittman TB, Shih YH, Strekalov DV, Sergienko AV. Phys Rev A 1995;52:R3429.
[17] Valencia A, Scarcelli G, Dangelo M, Shih YH. Phys Rev Lett 2005;94:063601.
[18] Mandel L. Phys Rev A 1983;28:929–43.
[19] Agafonov IN, Chekhova MV, Iskhakov TSh, Penin AN. Phys Rev A 2008;77:053801.
[20] Liu JB, Shih YH. Phys Rev A 2009;79:023819.
[21] Zhou Y, Simon J, Liu JB, Shih YH. Phys Rev A 2010;81:043831.
[22] Liu JB, Zhou Y, Zheng HB, Chen H, Li FL, Xu Z. Phys Opt 2014;1412. 2308v2.
[23] Wang RM, Pargorn P, Raza F, Ahmed I, Wang HX, Zhang YP. Laser Phys Lett 2018;15:085401.
[24] Li CB, Xu MY, Jiang WQ, Wang SQ, Luo ZQ, Li BW, Raza F, Zhang YP. Laser Phys 2018;28. 115404.
[25] Tang HJ, Ahmed I, Puttapirat P, Wu TH, Lan YW, Zhang YP, Li EL. Phys Chem Chem Phys 2018;20:5721–5.